

Short-Term Plasticity Based Network Model of Place Cells Dynamics

Sandro Romani,^{1,2,3*} and Misha Tsodyks^{1,2}

ABSTRACT: Rodent hippocampus exhibits strikingly different regimes of population activity in different behavioral states. During locomotion, hippocampal activity oscillates at theta frequency (5–12 Hz) and cells fire at specific locations in the environment, the place fields. As the animal runs through a place field, spikes are emitted at progressively earlier phases of the theta cycles. During immobility, hippocampus exhibits sharp irregular bursts of activity, with occasional rapid orderly activation of place cells expressing a possible trajectory of the animal. The mechanisms underlying this rich repertoire of dynamics are still unclear. We developed a novel recurrent network model that accounts for the observed phenomena. We assume that the network stores a map of the environment in its recurrent connections, which are endowed with short-term synaptic depression. We show that the network dynamics exhibits two different regimes that are similar to the experimentally observed population activity states in the hippocampus. The operating regime can be solely controlled by external inputs. Our results suggest that short-term synaptic plasticity is a potential mechanism contributing to shape the population activity in hippocampus. © 2014 The Authors. Hippocampus Published by Wiley Periodicals, Inc.

KEY WORDS: neural network; phase precession; hippocampus; place cells; sharp waves

INTRODUCTION

Neuronal population activity recorded in the hippocampus shows strikingly different profiles during different behavioral states of the animal. During exploration, the hippocampus exhibits a prominent oscillation in the 5–12 Hz range (theta frequency) (Vanderwolf, 1969; Buzsaki, 2002). During rest, this regular oscillatory profile switches to global irregular bursting activity (sharp-waves, SW) (Buzsaki, 1986). It is believed that SWs originate in the CA3 sub-field of the hippocampus (Buzsaki, 1989; Csicsvari et al., 2000), a region rich in recurrent collaterals. Artificial disruption of SWs impairs the acquisition of memory tasks, providing a causal link to memory

This is an open access article under the terms of the Creative Commons Attribution-NonCommercial-License, which permits use, distribution and reproduction in any medium, provided the original work is properly cited and is not used for commercial purposes.

¹Department of Neurobiology, Weizmann Institute of Science, Rehovot 76100, Israel; ²Department of Neuroscience, Center for Theoretical Neuroscience, College of Physicians and Surgeons, Columbia University, New York, New York; ³Department of Neuroinformatics, Donders Centre for Neuroscience, Radboud University, 6525 Nijmegen, The Netherlands.

Grant sponsor: European 7th Framework Programme SpaceBrain and Gatsby foundation, Human Frontier Science Program long-term fellowship, Israeli Science Foundation and Foundation Adelis..

*Correspondence to: Sandro Romani, Columbia University, College of Physicians and Surgeons, Department of Neuroscience, Kolb Research Annex, 1051 Riverside Drive, Unit 87, New York, NY, 10032-2695.

E-mail: sandro.romani@gmail.com

Accepted for publication 22 August 2014.

DOI 10.1002/hipo.22355

Published online 25 August 2014 in Wiley Online Library (wileyonlinelibrary.com).

consolidation (Ego-Stengel and Wilson, 2009; Girardeau et al., 2009; Jadhav et al., 2012).

Spiking activity observed in these two regimes also reveals profound differences. During exploratory behavior, cells preferentially fire at specific locations, the place fields (O'Keefe and Dostrovsky, 1971; O'Keefe, 1976). When the animal moves across a neuron's field, spikes are emitted at progressively earlier phases of the underlying theta rhythm (phase precession) (O'Keefe and Recce, 1993; Skaggs et al., 1996; Cei et al., 2014). During SWs, when the animal rests in a linear track or in a 2D environment, bursting activity occasionally spans sequences which cover—on a compressed time scale—a possible trajectory of the animal (Foster and Wilson, 2006; Diba and Buzsaki, 2007; Davidson et al., 2009; Karlsson and Frank, 2009; Gupta et al., 2010; Pfeiffer and Foster, 2013). We term these “virtual” runs non-local events (NLEs), since neural activity is not confined to represent the current location of the animal.

Is it possible to account for the regimes of neural dynamics described above with a single network? In this contribution we propose a neural network model of hippocampus that can exhibit both activity regimes. Our model rests on the observation that place selectivity as well as NLEs appears as spatially coherent activity patterns on the map defined by the place fields of the neurons. We therefore construct a recurrent network model of CA3 that can maintain spatially localized activity “bumps” (Tsodyks and Sejnowski, 1995). We assume that the map of the environment is stored in the strengths of synaptic connections, which depend on the distance between place fields of the corresponding neurons. Recurrent connections in the network are endowed with short-term synaptic depression (STD) that generates a movement of the bump accounting for NLEs (York and van Rossum, 2009). Depending on external inputs, networks with STD can also produce a burst-like behavior that is similar to SWs (Tsodyks et al., 2000; Loebel and Tsodyks, 2002).

MATERIALS AND METHODS

A basic unit of the network represents a population of neurons with highly overlapping place fields. Unit i is described by the firing rate at time t , $m_i(t)$, which follows the dynamics

$$\tau \dot{m}_i(t) = -m_i(t) + f(I_i^R(t) + I_i^E(t)).$$

$f(I) = \alpha \log(1 + e^{I/\alpha})$ is an f-I curve with an exponential sub-threshold tail and a linear supra-threshold

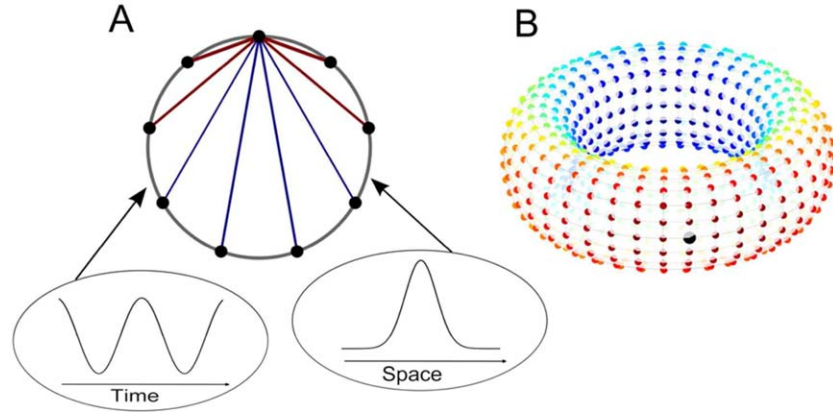


FIGURE 1. The network model. **A:** Units (black dots) are arranged on a map of a circular environment. Connections (lines) between units are strong (thick) and excitatory (red) for units with close place fields positions. At longer distances, connections become inhibitory (blue). In addition to this synaptic structure, short-term synaptic depression is present at every synapse; synaptic weights are modulated by the fraction of available resources that are depleted by the presynaptic activity (see Materials and Meth-

ods). The network receives a uniform oscillatory input (theta modulation) and a spatially tuned input. **B:** Toroidal environment. Units (dots) are arranged on a torus. Synaptic weights values from the black unit are color-coded. The warm-cold color gradient corresponds to a smooth change from excitatory to inhibitory effects. [Color figure can be viewed in the online issue, which is available at wileyonlinelibrary.com.]

component. The input current to unit i , is a sum of a recurrent $I_i^R(t)$ and an external contribution $I_i^E(t)$. The recurrent contribution to the current is

$$I_i^R(t) = \frac{1}{N} \sum_{j=1}^N W_{ij} m_j(t) x_j(t),$$

where the sum extends over the N units in the network. The synaptic strength W_{ij} depends on the geometry of the environment and will be specified in each case below. The dynamic variable $x_i(t)$ represents the depression strength of the connections from the pre-synaptic unit i to all its post-synaptic neighbors. This variable follows the dynamics (Tsodyks and Markram, 1997; Tsodyks et al., 1998)

$$\dot{x}_i(t) = \frac{1 - x_i(t)}{\tau_R} - U x_i(t) m_i(t),$$

where τ_R is the time constant of recovery from synaptic depression, and U is the fraction of utilized synaptic resources released by each spike (release probability). The external current contains three terms

$$I_i^E(t) = I + I_\Theta \cos(2\pi f_\Theta t) + I_L g_i(t).$$

I is a spatially uniform and stationary current. The second term is a theta-modulated input with frequency f_Θ and amplitude I_Θ . The last term is a place specific input, with amplitude I_L and a unit-dependent factor $g_i(t)$ that will be specified on a case-by-case basis below, depending on the geometry of the environment.

The Circular Environment

For simplicity, and in order to avoid boundary effects we first consider a network encoding a circular environment. A unit i is characterized by a place field at angle $\theta_i \in [0, 2\pi)$ in a circular arena (Fig. 1A). The place field locations are equally spaced on the circular arena.

The synaptic strength W_{ij} depends on the distance between the locations assigned to the units, excitatory for nearby locations and inhibitory if far apart (see Fig. 1):

$$W_{ij} = J_1 \cos(\theta_i - \theta_j) - J_0,$$

where J_1 measures the strength of the map-specific interaction and J_0 corresponds to a uniform feedback inhibition. Note that the synaptic structure in the model is an assumption, which has not been verified (nor falsified) in experimental studies. This form of interaction promotes the formation of spatially coherent activity (a “bump”) on the map (Amari, 1977; Ben-Yishai et al., 1995; Tsodyks and Sejnowski, 1995; Seung, 1996; Hansel and Sompolinsky, 1998). The place specific input is

$$g_i(t) = \cos(\theta_i - \theta_L(t)).$$

This input peaks at the location of the simulated animal $\theta_L(t)$ (Fig. 1A), which could correspond to an input from medial entorhinal cortical grid cells (Fyhn et al., 2004; Hafting et al., 2005).

The network parameters used are: $\tau = 10$ ms, $J_1 = 30$, $J_0 = 15$, $\tau_R = 0.8$ s, $U = 0.8$, $f_\Theta = 10$ Hz, $\alpha = 1$ Hz, $N = 100$. Parameters for the external currents can be found in Table 1.

Multiple Circular Environments

Each unit i in the network is characterized by a binary vector of selectivity for the K circular environments, ξ_i^k ,

TABLE 1.

Parameters for the External Inputs

	I (Hz)	I_L (Hz)	I_Θ (Hz)
NLEs (Fig.2)	-1	0	0
NLEs in multiple environments (Fig. 3)	0	0	0
NLEs with spatially tuned input (Fig. 4)	-1.1	0.15	0
Phase Precession (Figs. 5 and 6)	-7	15	8
T-Maze—Moving input (Figs. 7C,D, first 5 s)	10	20	12
T-Maze—Stationary input (Figs. 7C,D, last 3 s)	20	10	10
NLEs—spatial input—2D (Figs. 8A and 9)	-1.5	0.5	0
Phase Precession—2D (Figs. 8B and 9)	-7	15	5

where $i=1..N$, $\mu=1..K$. If the unit is selective for environment μ (i.e., the unit participates to the encoding of that environment) then $\xi_i^\mu=1$, or 0 otherwise (e.g., Solstad et al., 2014). Selectivity is assigned randomly, with the constraint that $\sum_i \xi_i^\mu = fN$, where f determines the fraction of units selective for any given environment. Each unit is also characterized by the vector of place field locations in the K circular environments, θ_i^μ [see e.g., (Battaglia and Treves, 1998; Romani and Tsodyks, 2010)].

The synaptic weights are defined as

$$W_{ij} = \frac{1}{f} \sum_{\mu=1}^K \xi_i^\mu \xi_j^\mu [J_1 \cos(\theta_i^\mu - \theta_j^\mu) - J_0].$$

The place field locations of the units selective for an environment are a random permutation of equally spaced place field locations in a circular environment. The place specific input is absent in this case, as we only consider the intrinsic dynamics of the network.

The network parameters used are: $J_1=25$, $J_0=23$, $N=300$, $f=0.3$, $K=3$. The remaining network parameters are the same of the previous section. Parameters for the external currents can be found in Table 1.

The T-Maze Environment

The T-maze is described by two 1D segments, representing the stem and branches, in a 2D plane. Setting the intersection point at the origin of the plane, a point \mathbf{p}_i on the maze is described by $\mathbf{p}_i=(x_i,0)$ where $x_i \in [-\pi,0)$ (stem, horizontal segment) or $\mathbf{p}_i=(0,y_i)$, $y_i \in [-\frac{\pi}{2},\frac{\pi}{2}]$ for the branches (vertical segment, see Fig. 7A). Similarly to the circular map case, units are equally spaced on the maze. The synaptic weight between a pair of units decays exponentially with the distance between their place field locations (Tsodyks et al., 1996)

$$W_{ij} = J_1 e^{-\frac{d(\mathbf{p}_i, \mathbf{p}_j)}{\lambda_I}} - J_0.$$

The function $d()$ is the Euclidean distance in 2D, $d(\mathbf{p}, \mathbf{p}') = \sqrt{(p_x - p_x')^2 + (p_y - p_y')^2}$, and λ_I sets the spatial scale of the interaction (see Fig. 7B).

The place specific input is described by

$$g_i(t) = e^{-\frac{d(\mathbf{p}_i, \mathbf{p}_L(t))}{\lambda_E}}.$$

This input decays exponentially around the location of the virtual animal $\mathbf{p}_L(t)$, with a spatial scale dictated by λ_E . For the simulations shown in Figures 7C,D, the peak of the spatial input $\mathbf{p}_L(t)$ moves with a constant speed on the stem of the T-maze for 5 s, and then remains constant for 3 s.

The network parameters used are: $J_1 = \frac{40}{U}$, $J_0 = \frac{30}{U}$, $U = 0.6$, $f_\Theta = 8$ Hz, $\lambda_I = 0.3$, $\lambda_E = 0.4$, $N = 1000$. The remaining network parameters are as in the section describing the circular environment. Parameters for the external currents can be found in Table 1.

The Toroidal Environment

For the case of a network storing a map of a toroidal environment, unit i is characterized by two angles, (θ_i^1, θ_i^2) (Fig. 1B). The synaptic interaction has the form (Romani and Tsodyks, 2010)

$$W_{ij} = J_1 [\cos(\theta_i^1 - \theta_j^1) + \cos(\theta_i^2 - \theta_j^2)] - J_0$$

and the spatially tuned external input is

$$g_i(t) = [\cos(\theta_i^1 - \theta_{L,1}(t)) + \cos(\theta_i^2 - \theta_{L,2}(t))]$$

Parameters: $J_1 = 35$, $J_0 = 25$, $N = 1024$, the rest of parameters as in 1D case. Parameters for the external currents can be found in Table 1.

Note that for a given environment, all the network parameters are kept constant and only the external input parameters are varied to produce the different dynamical regimes described in Results. For a given regime, both the network and the external input parameters are varied depending on the environment. We did not attempt to search for network parameters that would allow us to keep the external input parameters fixed for a given regime in all environments.

RESULTS

Spatially Coherent Large Irregular Activity

Simulating the network storing a map of a circular environment with a constant uniform input (see Materials and Methods), we observed the emergence of a novel regime of intrinsic activity. For a range of inputs, the network produces elevated activity that is quickly terminated due to fast depression of synaptic transmission (Fig. 2A). A new period of elevated activity is generated after recovery of the depressed synapses. Because of lateral inhibition and local excitation, this activity involves only units with neighboring place field locations (Fig. 2B). Intermittently, a spatially coherent activity bump moves along the map, producing NLEs. The activity is

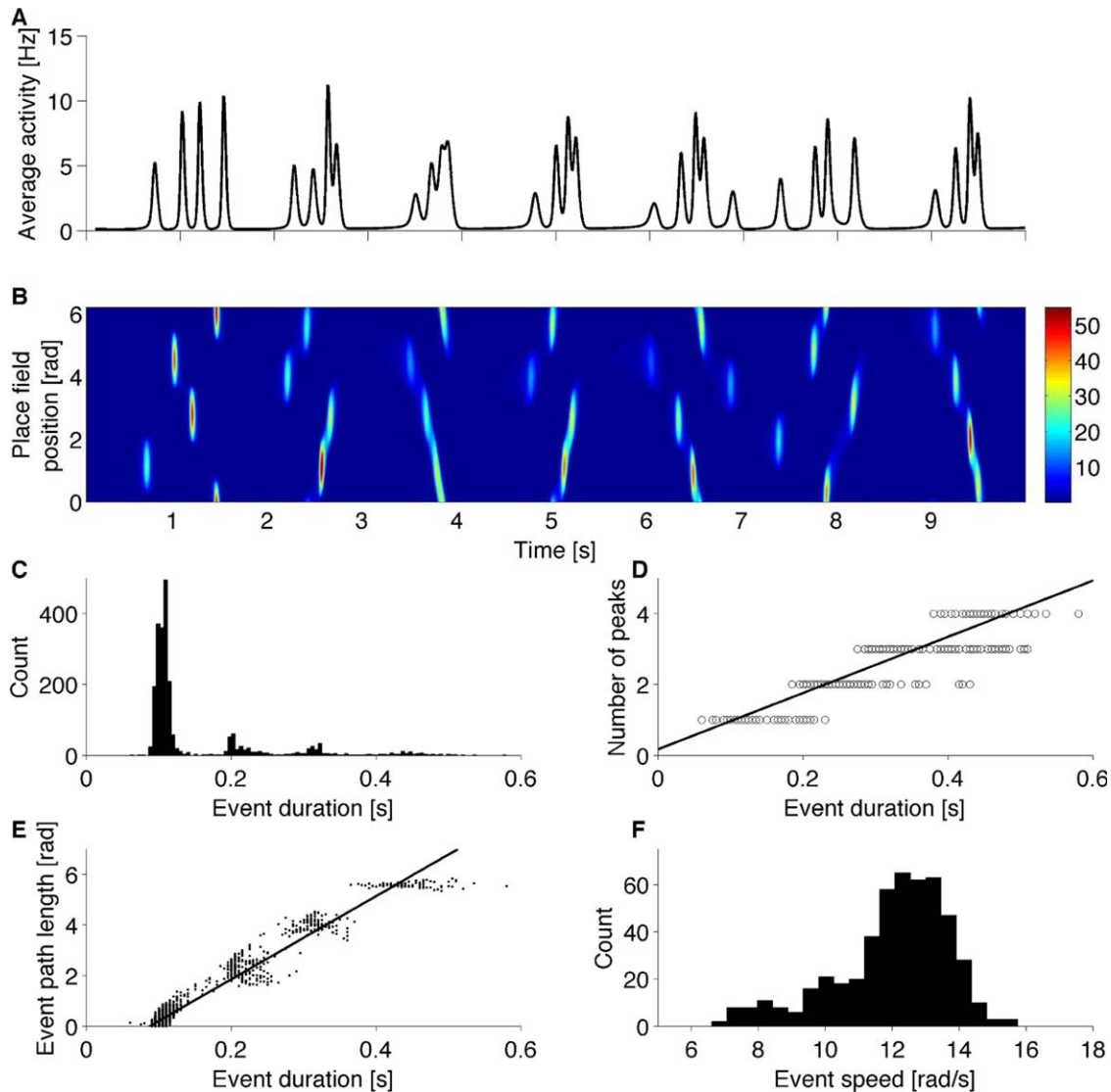


FIGURE 2. Network activity in the spatially coherent bursting regime. **A:** Average population activity from 10 s of simulated network dynamics in the case of constant uniform input. Periods of elevated activity are interspersed within periods of near silence, resembling multi-unit activity recordings from the rat hippocampus during immobility. **B:** Corresponding raster plot of single unit activity in the network. Units are orderly arranged in rows according to their place field position in the circular environment. The color code represents unit firing rates. Elevated activity is characterized by the transient activation of localized groups. **C:** Distribution of event duration. Events are extracted from the average population activity in a 1,000 s simulation (see text). **D:** The num-

ber of peaks in an event correlates with the duration of the event. One circle for each event (black line: linear regression, 7.9 peaks/s). **E:** Length of the traveled path during an event vs. event duration. Each dot corresponds to a burst event (black line: linear regression, 16.4 rad/s). Longer paths are observed for longer lasting events. The path length saturates at full circle length. **F:** Distribution of average bump speed during an event, computed from events with more than one peak (average 12 rad/s). See Materials and Methods for the parameters used in the simulation. [Color figure can be viewed in the online issue, which is available at wileyonlinelibrary.com.]

highly irregular, even though the equations representing the network dynamics are deterministic. This is due to the spatial localization of the neural activity: a bump emerging during a period of elevated activity locally alters the spatial profile of synaptic depression, which in turn influences the timing and localization of subsequent activity. In order to better characterize the network dynamics we performed a longer simulation (1,000 s). Following (Davidson et al., 2009), burst

events were defined as contiguous epochs of average population activity above a certain threshold (taken as activity averaged across neurons and the whole simulation period). A total of 2,275 burst events were identified, ranging from ~ 100 ms to ~ 500 ms duration (Fig. 2C). The average population activity is multi-peaked; in our network the fraction of burst events with 1 to 4 peaks is 78%, 12%, 8%, and 2%, respectively. The number of peaks in an event is growing with the

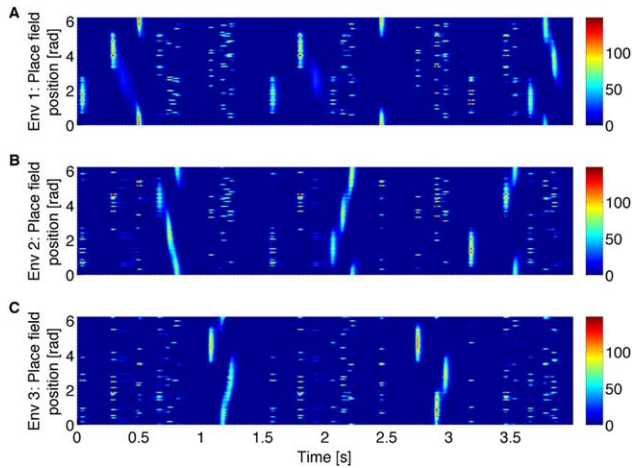


FIGURE 3. Bursting regime in a network storing multiple maps. **A:** Raster plot of single unit activity during 4 s of simulated dynamics with constant uniform input. Units are orderly arranged in rows according to their place field position in the first circular environment. All the units selective for environment 1 (30% of the total number of units) are included in the raster plot. Color code, unit firing rates. Periods of elevated activity are characterized by the activation of either localized groups or spatially incoherent subsets of units (B,C) As in (A), for environments 2 and 3. Note that spatially incoherent activity in one of the maps occurs whenever localized groups of neurons are active in another map. See Materials and Methods for the parameters used in the simulation. [Color figure can be viewed in the online issue, which is available at wileyonlinelibrary.com.]

event duration (Fig. 2D). Note that the duration of a single peaked burst event, ~ 100 ms, is comparable with the experimentally observed duration of a single SW event (Foster and

Wilson, 2006). Each peak in a burst event contributes ~ 100 ms to the total duration of the event, accounting for the structure observed in Figure 2C. These results are comparable to the experimental finding of chains of SWs in rodents exposed to long linear tracks (Davidson et al., 2009, Gupta et al., 2010), with an experimentally estimated number of ~ 10 SWs/s, compared with the model outcome of 7.9 peaks/s (Fig. 2D). The path length traveled by the bump increases with the duration of the event (Fig. 2E). Some of the burst events, but not all them, contain NLEs (path length > 0). NLEs occur typically, but not only, during burst events with two or more peaks. The distribution of average propagation velocity during events with more than one peak is unimodal, with a characteristic speed of ~ 12 rad/s (Fig. 2F), which can account for the close to linear relationship between path length and duration seen in Figure 2E.

Spatially Coherent Large Irregular Activity in Multiple Environments

One of the hallmarks of place cells activity in the hippocampus is the ability to code for spatial locations in multiple environments. For instance, when exposed to two distinct environments of similar shape, most place cells are active in only one environment, while the minority active in both environments exhibits place fields at different spatial locations, a phenomenon called global remapping (see e.g., Leutgeb et al., 2005). In this scenario, NLEs can be observed in both maps (Karlsson and Frank, 2009). To test whether the network model can qualitatively account for these observations, we stored the maps of three circular environments in the strength

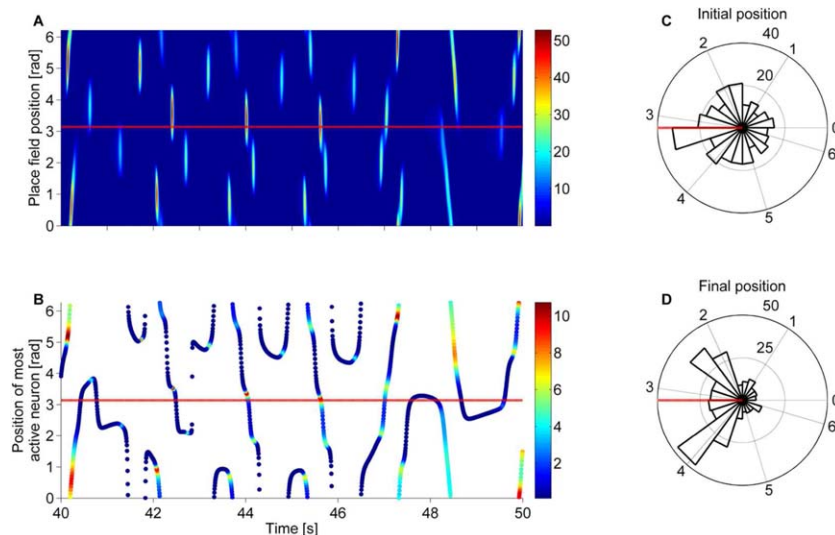


FIGURE 4. Activity of the network with spatially tuned input. The same network of Figure 2 but receiving a spatially tuned input around location π in the circular environment, representing the current location of the animal. **A:** Dynamics of network activity (color coded) shows moving spatially coherent activity bumps. Red line, location of the peak of the external input. **B:** Position of the maximally active unit in the network at every time-step. The

color code denotes the population averaged activity. Red line as in (A). **C:** Circular histogram of starting locations for burst events containing more than one peak in the average population activity. NLEs preferentially originate near the location biased by the spatially selective input (red line). **D:** Histogram of stopping locations for the events considered in (C). [Color figure can be viewed in the online issue, which is available at wileyonlinelibrary.com.]

of synaptic connections (see Materials and Methods). We observed the emergence of an irregular regime of activity in a network receiving a constant uniform input. Periods of elevated activity are sometimes characterized by activation of units with nearby place field locations in one of the maps (see e.g., the first 500 ms in Fig. 3A). In contrast with the dynamics that results from a network storing a single map, some periods of elevated activity are characterized by spatially unstructured patterns of units' activation (e.g., Fig. 3A, from 500 ms to 1 s). The unstructured activity results from spatially coherent activity occurring in other maps; A fraction of the units whose activity is spatially localized in one map, also participates to the encoding of other maps, where their activity appears unstructured (e.g., Figs. 3A,B, from 500 ms to 1 s). Within 4 s of network dynamics, spatially coherent activity and NLEs emerge in all three maps (Fig. 3). Note that there are no instances of spatially localized activity in more than one map simultaneously, due to global feedback inhibition.

Nonlocal Activity With Selective Spatial Input

Based on the similarity between the network behavior and the hippocampal activity during rest, we propose that the novel regime of intrinsic network activity described above corresponds to the experimentally observed NLEs. To establish a tighter link with the experimental observations, we add a place-specific input to the network pointing to a certain location on the map. This input provides information about the current location of the animal. The increased current to the units with place fields close to the position of the animal, biases the starting location of the moving bump on the map, as shown in Figures 4A–C. NLEs typically terminate at a short distance from the current location of the simulated animal (Fig. 4D), sometimes after travelling almost one full circle.

Place Fields and Phase Precession

When the animal is just entering a place field, the first spikes are emitted at the late phase of the ongoing theta rhythm, which is approximately the same for all cells. Subsequent spikes precess toward earlier phases of the theta cycle as the animal traverses a place field. One immediate implication of phase precession is the formation of “theta-sequences” in a population of place cells (Skaggs et al., 1996). Indeed, consider two place cells with overlapping place fields: when the animal moves from the first to the second field and its current location is in the overlapping region of the fields, the first cell will fire earlier than the second one within each theta-cycle, resulting in a wave of place cells activity which propagates towards the direction of motion of the animal. This effect has been recently observed experimentally with multi-unit recordings (Foster and Wilson, 2007; Davidson et al., 2009).

In our network, theta sequences emerge due to a combination of a moving place-specific input and spatially uniform oscillatory input at theta frequency (10 Hz), which could represent the input from the medial septum or entorhinal cortex (Buzsaki, 2002) (Fig. 5). The time course of network activity in Figure 5A,B shows that during each theta cycle, an activity

bump emerges, peaked at the neurons with the place fields centered near the current position of the animal (see Zugaro et al., 2004 for experimental evidence of extrahippocampal location reset at the beginning of a theta cycle). The bump subsequently propagates towards the direction of motion of the animal and then disappears at the phase of the theta cycle when inhibition is at its maximum. The packet of activity does not propagate backward, since the recent passage through the just visited locations excited the corresponding place units, thus temporarily depressing the connections between them. Hence, the packet of activity propagates towards unvisited locations.

This mechanism of phase precession is similar to an earlier network model based on asymmetric recurrent connections (Tsodyks et al., 1996), but in the current model theta sequences are generated by STD, hence asymmetry is not required. The absence of hard-wired asymmetry allows the model to produce theta sequences propagating along the direction of motion of the place-specific input, irrespective of its forward or backward direction. Hence the model results account for the experimental evidence of bi-directional theta sequences in one-dimensional environments (Ceï et al., 2014).

Single unit activity shows a shift of peak firing from the end of the cycle at the entrance of the field, to the beginning of the cycle while the simulated animal is leaving the place field (Fig. 5C). Phase precession is evident also from the firing rate map in the phase-position space (Fig. 5D). As in (Tsodyks et al., 1996), the intrinsic speed of propagation of the bump during a theta cycle is independent of the speed of the moving animal, thus ensuring a tighter correlation between phase and position, rather than phase and time spent in the place field (Fig. 6), in agreement with experimental results (O'Keefe and Recce, 1993). The circular-linear correlation between theta phase and position estimated from the data shown in Figure 6B is -0.14 , comparable with experimental results (Huxter et al., 2008). However, the range of precession, defined as the difference between the average firing phases on field entry (10% of the entire field) and field exit, is 65° . The observed range of precession is closer to 180° (Harris et al., 2002; Huxter et al., 2008). Note that a theta-modulated input is not necessary in order to obtain place specific firing. A strong selective spatial input alone is sufficient to stabilize the place field, accounting for the observation of place cell firing without theta-modulation in bats (Ulanovsky and Moss, 2007; Yartsev and Ulanovsky, 2013).

Activity Sweeps During Ongoing Theta Modulation

Another occurrence of NLEs was observed during alert immobility accompanied by theta oscillations. When an animal temporarily stops at the turning point of a T-maze, the reconstructed position showed alternating sweeps along the unvisited branches of the T-maze (Johnson and Redish, 2007).

We observed a similar behavior in a network encoding a map of a T-maze composed of two segments representing the stem and the branches (Fig. 7A). The maze is stored in the

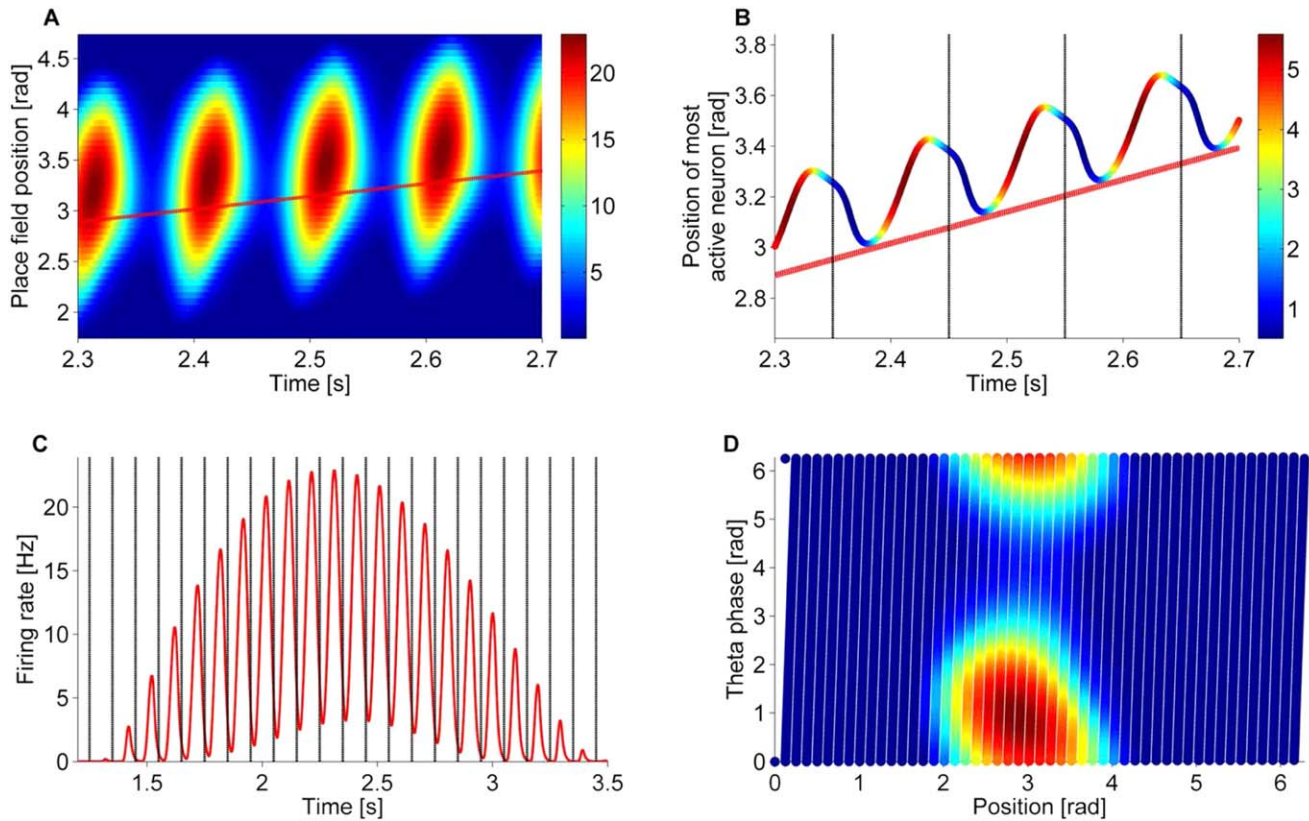


FIGURE 5. Phase precession in the presence of a moving spatially tuned input and global theta-modulation. **A:** 400 ms of network dynamics from a longer simulation in which the animal traveled the whole circular arena in 5 s. Red line, location of the animal. **B:** Time course of the bump position, identified by the preferred location of the maximally active unit. Vertical lines marks the times of minimal theta input. Color-code denotes average population activity, red line as in (A). **C:** Instantaneous firing rate of the unit with place field at π during the constant speed

run. Note the precession of firing peaks to earlier phases within theta periods. **D:** Color-coded firing rate of the same unit as a function of the theta-phase and position in the environment [color scale as in (A)]. Each dot corresponds to the position of the virtual animal and the phase of the external theta-modulated input at a given time point during the run (phase 0, maximal external input). [Color figure can be viewed in the online issue, which is available at wileyonlinelibrary.com.]

synaptic weights between pairs of units, which depend on 2D Euclidean distance between the corresponding fields on the map (Fig. 7B; see Materials and Methods for details). We simulated the network dynamics with a moving spatially tuned input in the presence of theta modulation to mimic a 5-s run along the stem of the maze (Figs. 7C,D). We assume that during the subsequent 3-s period of alert immobility, both spatially tuned input and theta-modulated inputs have reduced amplitude. Under these conditions, the network shows alternating sweeps of activity “exploring” the two branches (Figs. 7C,D). The network does not exhibit backward activity sweeps on the stem of the T-maze, because synapses connecting corresponding units were depressed when the animal moved along the stem.

Dynamics in Two Dimensional Environments

So far we considered the network representing a 1D environment, where most of the cells only fire in one direction (McNaughton et al., 1983). We now extend our model to 2D

environments, such as those used in random-foraging experiments, where place fields are nondirectional (Muller and Kubie, 1987; Skaggs et al., 1996; Huxter et al., 2008; Pfeiffer and Foster, 2013; Jeewajee et al., 2014).

For technical reasons, in order to avoid effects of the boundary, we considered an environment with opposite sides “glued” together, i.e., a torus (Romani and Tsodyks, 2010) (see Materials and Methods for details). We observed that the novel regime of irregular activity characterized by spatially coherent activity moving along the map is maintained also in this case. By numerically solving the network dynamics over a long period of time, we observed NLEs preferentially starting closer to the current position of the animal, but ending in random locations (Fig. 8A). To explore phase precession on the torus, we started with a straight run along one of the circles defining the torus. The activity bump grew and disappeared within a theta cycle, while moving toward the direction of motion of the animal, similar to the behavior observed in the circular environment (not shown). As in the 1D case, this movement results in phase precession. The correlation between phase and

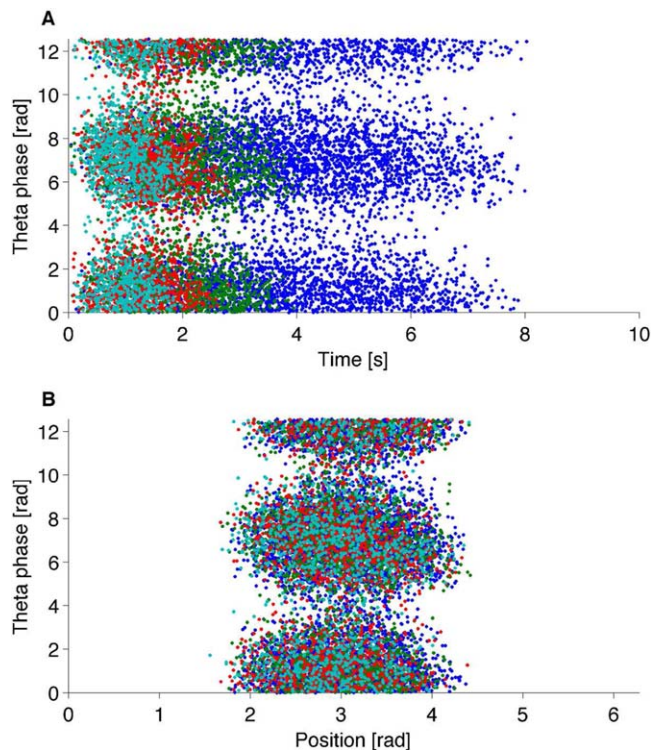


FIGURE 6. Correlation of firing phase with time and position. **A:** Spikes (dots) were generated from 100 realizations of a Poisson process, with rate given by the activity of a neuron with place field at π during a constant speed run in the circular environment. Different colors denote four different speeds, with speeds equally spaced from $\frac{2\pi}{20}$ to $\frac{2\pi}{5}$ rad/s (from slow to fast: blue, green, red, cyan). Theta phase at spike emission is plotted versus the time after entering the neuron place field. Phase precession is observed for any given speed, but is hardly noticeable when considering all the runs together. **B:** The same spikes as in (A) but with theta phase at the time of each spike emission plotted versus the position of the virtual animal. Phase precession does not depend on running speed. The circular-linear correlation is -0.14 . In both panels spikes are slightly randomly displaced on the x -axis to avoid artifacts due to the absence of variability in theta modulation. [Color figure can be viewed in the online issue, which is available at wileyonlinelibrary.com.]

position is -0.15 , similar to the correlation obtained from straight runs in experiments (Huxter et al., 2008; Jeewajee et al., 2014). As in the 1D case, the average range of precession is limited to 66° (not shown). We also observed phase precession when simulating an animal traveling along a correlated random walk at constant speed (Fig. 8B).

Predictions of the Model

The main prediction results from the presence of short-term synaptic depression dynamics. We have shown that depression of synaptic transmission between units with place fields recently traversed by the animal prevents backward propagation of the bump of activity (i.e., during phase precession, or for the activity sweeps in the T-maze). This suggests that, in 2D,

NLEs should preferentially avoid the recent path traveled by the animal, at least during SW occurring shortly after the animal stops (Fig. 9). This prediction could be tested with a careful analysis of the experimental results in (Pfeiffer and Foster, 2013). A second prediction is related to the velocity of the animal and its influence on the level of depression on synapse. In the T-maze, when the animal is approaching the decision point at elevated speed, the backward sweeps should be more probable since the synapses had less time to reach a highly depressed state. The few backward sweeps observed in the experiment of (Johnson and Redish, 2007) could be analyzed in order to test this prediction.

DISCUSSION

We proposed a neural network model that accounts for the diverse range of hippocampal activity states. The model has two major ingredients: the recurrent connections encode a map of the environment, and synaptic transmission exhibits short-term depression. We observed a novel regime of network activity in the form of temporally irregular bursts of spatially coherent subsets of neurons, occasionally moving along the neural map. Due to the assumed pattern of recurrent connections, the intrinsic activity of the network is shaped by the stored map of the environment, resembling the spontaneous emergence of the orientation maps observed in the visual cortex (Kenet et al., 2003). This novel form of network activity also accounts for the activity replays observed during slow-wave sleep (Wilson and McNaughton, 1994; Lee and Wilson, 2002) and, in line with experimental findings, supports the hypothesis that the intrinsic mode of operation of CA3 is bursting activity (Buzsáki, 1986). In the absence of oscillatory modulation the model also accounts for place selectivity without phase precession (Ulanovsky and Moss, 2007; Yartsev and Ulanovsky, 2013). An additional oscillatory modulation controls the movement of the activity packet during each cycle, resulting in phase precession. Manipulation of the input when the simulated animal is steady produces escaping activity that resembles the observed sweeps at decision points. In 2D environments, the model exhibits phase precession and predicts NLEs that preferentially avoid the recent trajectory of the animal during the first SWs following immobility. The emergence of NLEs in the model could potentially account for activity “preplays” (Dragoi and Tonegawa, 2011; 2013), where sequences of place cells recorded during exploration of a novel environment were pre-played during SWs preceding the experience. NLEs generated by a network storing multiple environments could be primed for use in subsequent exploratory behavior, when a map of the novel environment can be stored via Hebbian plasticity mechanisms.

It is widely believed that cholinergic modulation plays a major role in the switching between dynamic regimes, but the observation of theta activity interspersed with SWs (O’Neill

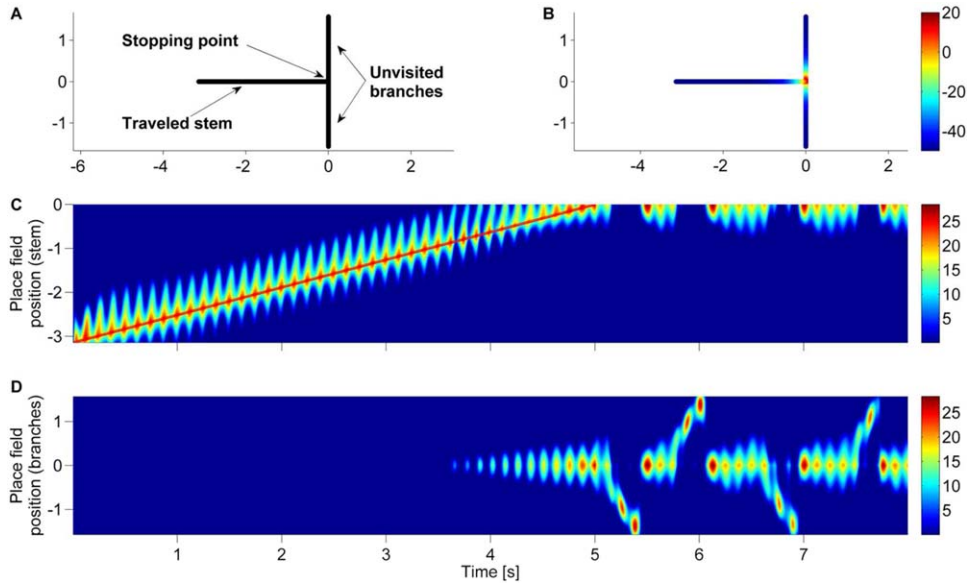


FIGURE 7. Activity sweeps in a T-Maze. **A:** Geometry of the environment and the animal's trajectory. Two segments of equal length are used as the map of a T-maze. Units have place fields arranged on a regular grid on the map. During the simulation, the virtual animal runs for 5 s from the left-most point on the maze stem to the stopping point at the crossing, followed by additional 3 s at the crossing. **B:** Synaptic weights (color coded) of recurrent connections from the unit at the stopping point to the rest of the network. **C:** Network activity on the stem of the T-maze. Units are sorted according to their place field position on the horizontal segment of the map. Firing rate is color coded. Red

line: movement of the spatial input during the first 5 s. At rest, no sweeps of activity are observed on the stem. **D:** Network activity on the unvisited branches of the maze. Units sorted according to their place field position on the vertical segment. Units close to the crossing activate when the virtual animal approaches the stopping point at 5 s. For the remaining 3 s the average external input to the network is increased, while the amplitudes of the theta-modulated and spatially selective inputs are decreased. Sweeps of activity cover the unvisited regions of the segment. [Color figure can be viewed in the online issue, which is available at wileyonlinelibrary.com.]

et al., 2006) supports the assumption that switching can be a fast process occurring without the influence of neuromodulators. Since external currents control the different regimes of the network, opto-genetics tools could provide an effective way to probe the model dynamical regimes by depolarizing/hyperpolarizing CA3 neurons or directly manipulating its afferents.

The movement of the activity packet on the neural map caused by STD is an extension of previous recurrent network models of phase precession, where an asymmetry in the synaptic structure generates the movement of the packet (Tsodyks et al., 1996; Jensen and Lisman, 1996; Wallenstein and Hasselmo, 1997). This model has been shown to be consistent with the

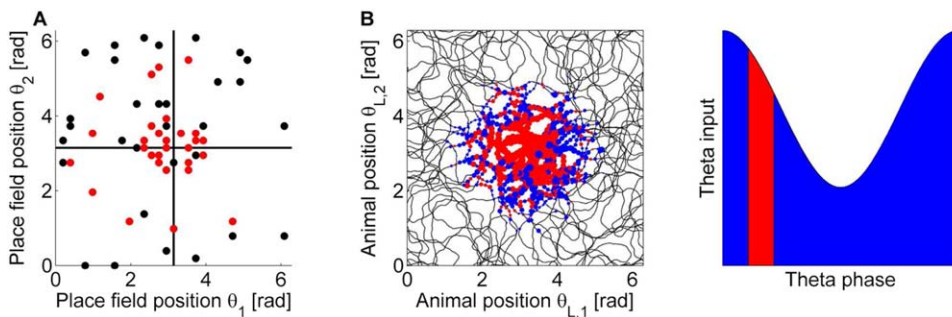


FIGURE 8. Local and nonlocal activity in a 2D environment. **A:** NLEs in a toroidal map, with a place specific input around the (π, π) location. Red and black dots denote respectively the location of origin and ending of the NLEs during identified bursts events from a simulation of 50 s (same method as for the 1D case). NLEs typically start close to the location imposed by the selective external input. NLEs terminate at locations covering the torus more uniformly. **B:** Phase precession in 2D. The curve represents the simulated trajectory of the animal (correlated random

walk with a constant speed of $\frac{2\pi}{5}$ rad/s, and 0.05 angular s.d.) in a run of 300 s. The firing rate (thresholded at 0.5 Hz) of the peaks of the unit with place field at (π, π) is size-coded, bigger dots correspond to higher firing rates. The color denotes the phase of the external theta-input at the time of the peaks in the firing rate. For illustration purposes, the phases are binarized (red and blue). [Color figure can be viewed in the online issue, which is available at wileyonlinelibrary.com.]

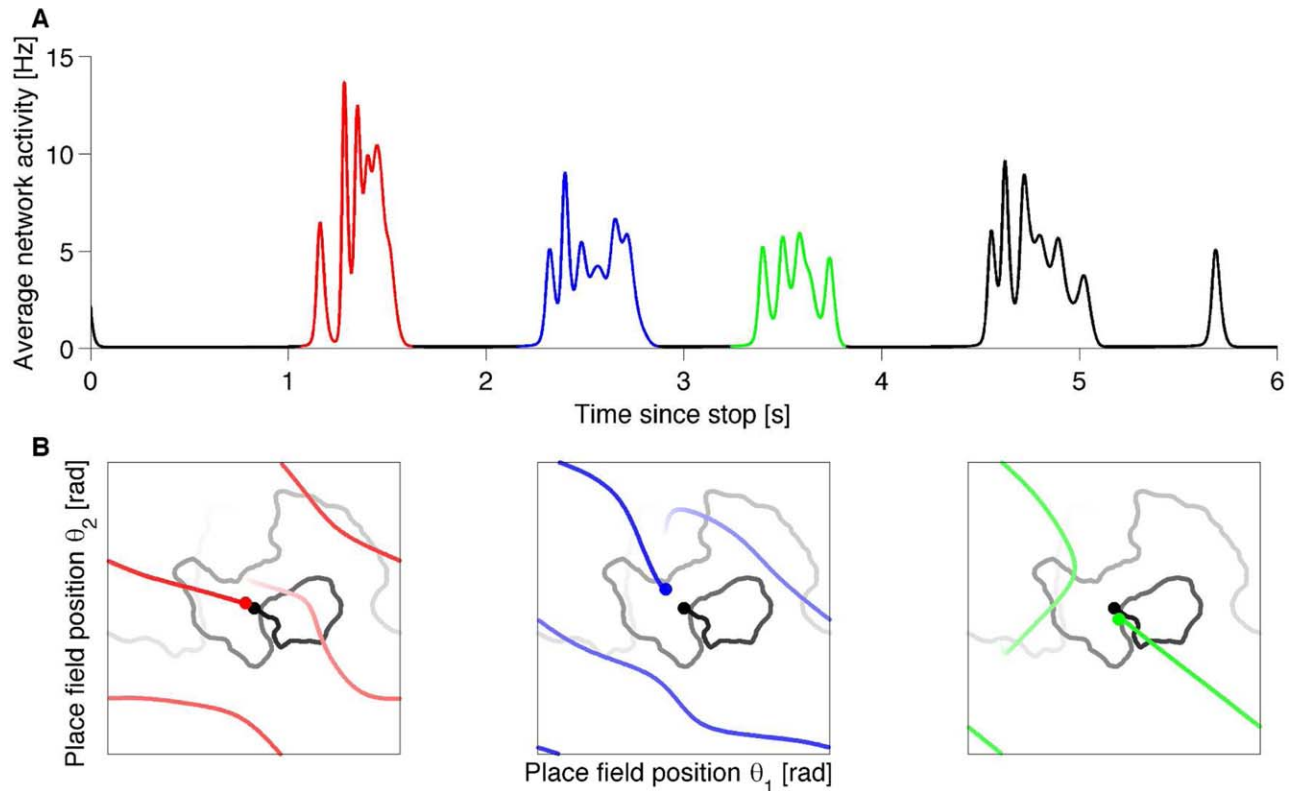


FIGURE 9. Properties of nonlocal activity in 2D environments. **A:** Network in the bursting regime after 20 s of simulated motion of the animal (correlated random walk as in Fig. 8). The chronological occurrence of the first three bursting events after the animal stops ($T=0$) is color coded (red, blue, and green, early to late). **B:** Three NLEs during the bursting events. The gray curve represents the simulated path of the animal; colored curves denote the path

traveled by the bump during the bursts. The black dot marks the position of the animal stop location, colored dots mark the initial location of the NLEs. The shading of the curves is a measure of the time passed from the animal stop, darker shading for times close to $T=0$. Note how the first two NLEs (red and blue) avoid the recent path of the animal. [Color figure can be viewed in the online issue, which is available at wileyonlinelibrary.com.]

experimental findings about phase precession, the robustness to transient perturbation of activity (Zugaro et al., 2004), and the intracellular signatures of place coding (Harvey et al., 2009; Romani et al., 2011). However, the model relies on the directionality of the neurons, and cannot account for phase precession in 2D, where place cells are not directional, or reverse phase precession in 1D during backward travel (Cei et al., 2014). In our model, the movement of the activity packet is caused by STD, hence connections can be symmetric. Strong STD has been indeed observed in CA3 synapses in vitro (Selig et al., 1999), but other studies report a mixture of short-term synaptic facilitation and depression (Miles and Wong, 1986). The behavior of the network with such connections, in the conditions we considered, is qualitatively similar to the one presented in the paper (not shown). Networks with mixed depressing/facilitating synapses have a richer repertoire of behaviors; a full description of the dynamical regimes of the network with depressing, facilitating, or mixed synapses, and the dependence of network behavior on internal and external parameters is outside the scope of the present contribution and will be presented in future studies.

This study shows that attractor networks with short-term synaptic plasticity in recurrent connections can account for a

wide range of experimental observations on hippocampal dynamics. We cannot exclude that additional or alternative dynamics at the single neuron or single synapse level may contribute to the observed hippocampal circuit dynamics. For instance, spike frequency adaptation in attractor networks has been shown to produce spontaneous movement of the activity packet (Hansel and Sompolinsky, 1996; Itskov et al., 2011; Azizi et al., 2013), and bursting activity in unstructured spiking networks (Gigante et al., 2007). Whether spike frequency adaptation alone could be sufficient to reproduce the results of our model, and how it would be possible to experimentally discriminate between the two alternatives, will be matter for future studies.

Several studies used facilitation mechanisms to generate firing sequences in models of hippocampal or entorhinal circuits (Leibold et al., 2008; Thurley et al. 2008; Navratilova et al., 2012). In (Leibold et al. 2008; Thurley et al., 2008) a facilitating excitatory input interacted with oscillating excitability in CA3, resulting in temporal compression of sequential activity, as in phase precession. In this class of facilitation models, phase precession results from feed-forward mechanisms, in contrast with the primary role of recurrent connections in our model.

In (Navratilova et al. 2012) path integration network model, a velocity specific input was used to generate an asymmetry in the network, responsible for the movement of the bump; neuronal facilitation (after-depolarization) contributed to resetting the bump at the beginning of a theta cycle, resulting in phase precession. In contrast, in our model, the asymmetry is generated with STD while the reset is achieved with a place-specific input.

It has been suggested that nonlocal hippocampal activity observed during sharp-waves in wakefulness and sleep contributes to memory consolidation. The model we propose exposes a potential mechanism for the generation of such activity, thus constituting an important first step towards the mechanistic understanding of memory encoding.

Our study shows that short-term synaptic plasticity allows the network to be effectively controlled by afferent inputs to produce vastly different dynamic activity regimes. This could be a way for the network to adapt its properties to specific computational demands associated with different behavioral states of the animal. We suggest that this flexibility could be a general feature of cortical networks.

Acknowledgments

The authors thank G. Buzsáki, E. Pastalkova, L. Abbott, and F. Battaglia for fruitful discussions. The authors thank O. Barak, J. Schmiedt, and S. Mark for comments on the manuscript. A. Rubin participated in the early phase of the project.

REFERENCES

- Amari SI. 1977. Dynamics of pattern formation in lateral-inhibition type neural fields. *Biol Cybernetics* 27:77–87.
- Azizi AH, Wiskott L, Cheng S. 2013. A computational model for replay in the hippocampus. *Front Comp Neurosci* 7.
- Battaglia FP, Treves A. 1998. Attractor neural networks storing multiple space representations: A model for hippocampal place fields. *Phys Rev E* 58:7738.
- Ben-Yishai R, Bar-Or RL, Sompolinsky H. 1995. Theory of orientation tuning in visual cortex. *Proc Natl Acad Sci USA* 92:3844–3848.
- Buzsáki G. 1989. Two-stage model of memory trace formation: A role for "noisy" brain states. *Neuroscience* 31:551–570.
- Buzsáki G. 1986. Hippocampal sharp waves: Their origin and significance. *Brain Res* 398:242–252.
- Buzsáki G. 2002. Theta oscillations in the Hippocampus. *Neuron* 33:325–340.
- Cei A, Girardeau G, Drieu C, El Kanbi K, Zugaro M. 2014. Reversed theta sequences of hippocampal cell assemblies during backward travel. *Nat Neurosci* 17:719–724.
- Csicsvari J, Hirase H, Mamiya A, Buzsáki G. 2000. Ensemble patterns of hippocampal CA3-CA1 neurons during sharp wave-associated population events. *Neuron* 28:585–594.
- Davidson TJ, Kloosterman F, Wilson MA. 2009. Hippocampal replay of extended experience. *Neuron* 63:497–507.
- Diba K, Buzsáki G. 2007. Forward and reverse hippocampal place-cell sequences during ripples. *Nat Neurosci* 10:1241–1242.
- Dragoi G, Tonegawa S. 2011. Preplay of future place cell sequences by hippocampal cellular assemblies. *Nature* 469:397–401.
- Dragoi G, Tonegawa S. 2013. Distinct preplay of multiple novel spatial experiences in the rat. *Proc Natl Acad Sci USA* 110:9100–9105.
- Ego-Stengel V, Wilson MA. 2009. Disruption of ripple-associated hippocampal activity during rest impairs spatial learning in the rat. *Hippocampus* 20:1–10.
- Foster DJ, Wilson MA. 2007. Hippocampal theta sequences. *Hippocampus* 17:1093–1099.
- Foster DJ, Wilson MA. 2006. Reverse replay of behavioural sequences in hippocampal place cells during the awake state. *Nature* 440:680–683.
- Fyhn M, Molden S, Witter MP, Moser EI, Moser M-B. 2004. Spatial representation in the entorhinal cortex. *Science* 305:1258–1264.
- Gigante G, Mattia M, Del Giudice P. 2007. Diverse population-bursting modes of adapting spiking neurons. *Phys Rev Lett* 98:148101.
- Girardeau G, Benchenane K, Wiener SI, Buzsáki G, Zugaro MB. 2009. Selective suppression of hippocampal ripples impairs spatial memory. *Nat Neurosci* 12:1222–1223.
- Gupta AS, Der Meer MAA, van; Touretzky DS, Redish AD. 2010. Hippocampal replay is not a simple function of experience. *Neuron* 65:695–705.
- Hafting T, Fyhn M, Molden S, Moser MB, Moser EI. 2005. Microstructure of a spatial map in the entorhinal cortex. *Nature* 436:801–806.
- Hansel D, Sompolinsky H. 1998. Methods in neuronal modeling: from synapse to networks. Koch C, Segev I, editors. Cambridge, MA: MIT Press.
- Harris KD, Henze DA, Hirase H, Leinekugel X, Dragoi G, Czurko A, Buzsáki G. 2002. Spike train dynamics predicts theta-related phase precession in hippocampal pyramidal cells. *Nature* 417:738–741.
- Harvey CD, Collman F, Dombeck DA, Tank DW. 2009. Intracellular dynamics of hippocampal place cells during virtual navigation. *Nature* 461:941–946.
- Huxter JR, Senior TJ, Allen K, Csicsvari J. 2008. Theta phase-specific codes for two-dimensional position, trajectory and heading in the hippocampus. *Nat Neurosci* 11:587–594.
- Itskov V, Curto C, Pastalkova E, Buzsáki G. 2011. Cell assembly sequences arising from spike threshold adaptation keep track of time in the hippocampus. *J Neurosci* 31:2828–2834.
- Jadhav SP, Kemere C, German PW, Frank LM. 2012. Awake hippocampal sharp-wave ripples support spatial memory. *Science* 336:1454–1458.
- Jeewajee A, Barry C, Douchamps V, Manson D, Lever C, Burgess N. 2014. Theta phase precession of grid and place cell firing in open environments. *Phil Transact Roy Soc B: Biol Sci* 369:20120532.
- Jensen O, Lisman JE. 1996. Hippocampal CA3 region predicts memory sequences: Accounting for the phase precession of place cells. *Learn Mem* 3(2-3):279–287.
- Johnson A, Redish AD. 2007. Neural ensembles in CA3 transiently encode paths forward of the animal at a decision point. *J Neurosci* 27:12176–12189.
- Karlsson MP, Frank LM. 2009. Awake replay of remote experiences in the hippocampus. *Nature Neurosci* 12:913–918.
- Kenet T, Bibitchkov D, Tsodyks M, Grinvald A, Arieli A. 2003. Spontaneously emerging cortical representations of visual attributes. *Nature* 425:954–956.
- Lee AK, Wilson MA. 2002. Memory of sequential experience in the hippocampus during slow wave sleep. *Neuron* 36:1183–1194.
- Leibold C, Gundlfinger A, Schmidt R, Thurley K, Schmitz D, Kemper R. 2008. Temporal compression mediated by short-term synaptic plasticity. *Proc Natl Acad Sci USA* 105:4417–4422.
- Leutgeb S, Leutgeb JK, Barnes CA, Moser EI, McNaughton BL, Moser MB. 2005. Independent codes for spatial and episodic

- memory in hippocampal neuronal ensembles. *Science* 309:619–623.
- Loebel A, Tsodyks M. 2002. Computation by ensemble synchronization in recurrent networks with synaptic depression. *J Comput Neurosci* 13:111–124.
- McNaughton BL, Barnes CA, O'Keefe J. 1983 The contributions of position, direction, and velocity to single unit activity in the hippocampus of freely-moving rats. *Exp Brain Res* 52:41–49.
- Miles R, Wong RK. 1986. Excitatory synaptic interactions between CA3 neurones in the guinea-pig hippocampus. *J Physiol* 373:397.
- Muller RU, Kubie JL. 1987. The effects of changes in the environment on the spatial firing of hippocampal complex-spike cells. *J Neurosci* 7:1951–1968.
- Navratilova Z, Giocomo LM, Fellous JM, Hasselmo ME, McNaughton BL. 2012. Phase precession and variable spatial scaling in a periodic attractor map model of medial entorhinal grid cells with realistic after-spike dynamics. *Hippocampus* 22:772–789.
- O'Keefe J. 1976. Place units in the hippocampus of the freely moving rat. *Exp Neurol* 51:78–109.
- O'Keefe J, Dostrovsky J. 1971. The hippocampus as a spatial map. Preliminary evidence from unit activity in the freely-moving rat. *Brain Res* 34:171–175.
- O'Keefe J, Recce ML. 1993. Phase relationship between hippocampal place units and the EEG theta rhythm. *Hippocampus* 3:317–330.
- O'Neill J, Senior T, Csicsvari J. 2006. Place-selective firing of CA1 pyramidal cells during sharp wave/ripple network patterns in exploratory behavior. *Neuron* 49:143–155.
- Pfeiffer BE, Foster DJ. 2013. Hippocampal place-cell sequences depict future paths to remembered goals. *Nature* 497:74–79.
- Romani S, Sejnowski TJ, Tsodyks M. 2011. Intracellular dynamics of virtual place cells. *Neural Comput* 23:651–655.
- Romani S, Tsodyks M. 2010. Continuous attractors with morphed/correlated maps. *PLoS Comput Biol* 6:e1000869.
- Selig DK, Nicoll RA, Malenka RC. 1999. Hippocampal long-term potentiation preserves the fidelity of postsynaptic responses to presynaptic bursts. *J Neurosci* 19:1236–1246.
- Seung HS. 1996. How the brain keeps the eyes still. *Proc Natl Acad Sci USA* 93:13339–13344.
- Skaggs WE, McNaughton BL, Wilson MA, Barnes CA. 1996. Theta phase precession in hippocampal neuronal populations and the compression of temporal sequences. *Hippocampus* 6:149–172.
- Solstad T, Yousif HN, Sejnowski TJ. 2014. Place cell rate remapping by CA3 recurrent collaterals. *PLOS Comp Biol* 10:e1003648.
- Thurley K, Leibold C, Gundlfinger A, Schmitz D, Kempster R. 2008. Phase precession through synaptic facilitation. *Neural Comp* 20:1285–1324.
- Tsodyks MV, Markram H. 1997. The neural code between neocortical pyramidal neurons depends on neurotransmitter release probability. *Proc Natl Acad Sci USA* 94:719–723.
- Tsodyks MV, Skaggs WE, Sejnowski TJ, McNaughton BL. 1996. Population dynamics and theta rhythm phase precession of hippocampal place cell firing: a spiking neuron model. *Hippocampus* 6:271–280.
- Tsodyks M, Pawelzik K, Markram H. 1998. Neural networks with dynamic synapses. *Neural Comput* 10:821–835.
- Tsodyks M, Uziel A, Markram H. 2000. Synchrony generation in recurrent networks with frequency-dependent synapses. *J Neurosci* 20:RC50.
- Tsodyks M, Sejnowski TJ. 1995. Associative memory and hippocampal place cells. *Int J Neural Syst* 6:81–86.
- Ulanovsky N, Moss CF. 2007. Hippocampal cellular and network activity in freely moving echolocating bats. *Nat Neurosci* 10:224–233.
- Vanderwolf CH. 1969. Hippocampal electrical activity and voluntary movement in the rat. *Electroencephalography Clin Neurophysiol* 26:407–418.
- Wallenstein GV, Hasselmo ME. 1997. GABAergic Modulation of hippocampal population activity: Sequence learning, place field development, and the phase precession effect. *J Neurophysiol* 78:393–408.
- Wilson MA, McNaughton BL. 1994. Reactivation of hippocampal ensemble memories during sleep. *Science* 265:676–679.
- Yartsev MM, Ulanovsky N. 2013. Representation of three-dimensional space in the hippocampus of flying bats. *Science* 340:367–372.
- York L, vanRossum M. 2009. Recurrent networks with short term synaptic depression. *J Comp Neurosci* 27:607–620.
- Zugaro MB, Monconduit L, Buzsáki G. 2004. Spike phase precession persists after transient intrahippocampal perturbation. *Nat Neurosci* 8:67–71.